HHS Public Access

Author manuscript

Sci Transl Med. Author manuscript; available in PMC 2023 January 31.

Published in final edited form as:

Sci Transl Med. 2020 November 18; 12(570): . doi:10.1126/scitranslmed.abc1492.

Ectopic HCN4 expression drives mTOR-dependent epilepsy in mice

Lawrence S. Hsieh[1], **John H. Wen**[1], **Lena H. Nguyen**[1], **Longbo Zhang**[1], **Stephanie Getz**[1], **Juan Torres-Reveron**[1,†], **Ying Wang**[3], **Dennis D. Spencer**[1], **Angélique Bordey**[*,1,2]

[1]Department of Neurosurgery, Yale University School of Medicine, 333 Cedar Street, New Haven, CT 06520, USA

[2]Department of Cellular & Molecular Physiology, Yale University School of Medicine, 333 Cedar Street, New Haven, CT 06520, USA

[3]Emergency Department, Xiangya Hospital, Central South University, 87 Xiangya Street, Changsha, Hunan 410008, China.

Abstract

The causative link between focal cortical malformations (FCM) and epilepsy is well-accepted, especially among patients with focal cortical dysplasia type II (FCDII) and tuberous sclerosis complex (TSC). However, the mechanisms underlying seizures remain unclear. Using a mouse model of TSC- and FCDII-associated FCM, we showed that FCM neurons were responsible for seizure activity via their unexpected abnormal expression of the hyperpolarization-activated cyclic nucleotide-gated potassium channel isoform 4 (HCN4), which is normally not present in cortical pyramidal neurons after birth. Increasing intracellular cAMP concentrations, which preferentially affects HCN4 gating relative to the other isoforms, drove repetitive firing of FCM neurons but not control pyramidal neurons. Ectopic HCN4 expression was dependent on the mechanistic target of rapamycin (mTOR), preceded the onset of seizures, and was also found in diseased neurons in tissue resected from patients with TSC and FCDII. Finally, blocking HCN4 channel activity in FCM neurons prevented epilepsy in the mouse model. These findings suggest that HCN4 play a main role in seizure and identify a cAMP-dependent seizure mechanism in TSC and FCDII. Furthermore, the unique expression of HCN4 exclusively in FCM neurons suggests that gene therapy targeting HCN4 might be effective in reducing seizures in FCDII or TSC.

One Sentence Summary:

[*]To whom correspondence should be addressed: Angélique Bordey, Ph.D., Department of Neurosurgery, Yale University School of Medicine, 333 Cedar Street, FMB 422, New Haven, CT 06520-8082, Phone: 203-737-2515, Fax: 203-737-2159, angelique.bordey@yale.edu.

[†]present address: Department of Neurosurgery, University of Cincinnati Academic Health Center, 222 Piedmont Avenue, Suite 6200, Cincinnati, OH 45219, USA.

Author contributions: LH and AB designed the experiments. LSH performed the patch-clamp and EEG experiments and analysis, JW did most immunostaining, LHN did some HCN1-HCN3 immunostaining, the antibody validation using siRNA, and EEG analysis for the $HCN4^{NF}$ experiment, SG did some HCN4 immunostaining, and LZ performed some IUE. DS, JTR, WY, and LZ provided human tissue samples. AB, LH and LHN wrote the manuscript.

Competing interests: L.H. and A.B. are co-inventors on a patent application PCT/US2020/020994 entitled “methods of treating and diagnosing epilepsy”. Dr. Bordey is an unpaid consultant for the Tuberous Sclerosis Alliance and has been a paid consultant for AskBio, Inc.

A cAMP-dependent mechanism mediates seizures in mTOR disorders due to the ectopic expression of HCN4 channels in diseased neurons.

Introduction

Disorders caused by mutations in the mTOR pathway genes lead to mTOR hyperactivity, brain malformations, and life-long epilepsy in the majority of patients (1, 2). Among this group of disorders, FCD and TSC account for the largest population of children and young adults who undergo brain surgery to treat intractable epilepsy (3–5). Nearly two-thirds of these patients are refractory to treatment with antiepileptic drugs and experience life-long seizures, leading to a spectrum of neurocognitive and psychological disabilities (1). Upon failure of conventional antiepileptic drugs, surgical resection of the seizure foci or pharmacological inhibition of mTOR signaling in the case of TSC are the only available treatments for mTOR-dependent focal epilepsy, but neither option is fully effective (6, 7). Despite the identification of the molecular pathways dysregulated in TSC and FCDII and the pathological characteristics associated with seizures (3, 8, 9), the mechanism of epileptogenesis remains to be fully elucidated, although several hypotheses of epileptogenicity have been proposed. These include abnormal reorganization of the circuitry within and surrounding FCMs and abnormal electrophysiological properties of FCM neurons (4, 10–12). In addition, the exact site and the cell types responsible for epileptogenic activity in humans remain controversial as some studies have recorded epileptic discharges both inside and outside of FCMs whereas other studies have found FCMs to be electrically silent (12, 13). The lack of consensus on the site of seizure generation further reflects our poor understanding of the epileptogenic mechanisms, which has hampered the identification of therapeutic targets and more effective treatment options.

Using a mouse model of TSC and FCDII (14), we show here that silencing FCM neurons prevented the occurrence of seizures, suggesting that FCM neurons might be responsible for seizure activity. To identify how FCM neurons drove seizures, we obtained patch clamp recordings in FCM neurons and identified an abnormal expression of HCN4, which is not present in normal pyramidal neurons. Although FCM neurons were depolarized and hence closer to the threshold for action potential generation, they required more current injection than controls to reach that threshold due to the cells' increased size and intrinsic conductance. Consistent with the fact that HCN4 channels are the most cAMP sensitive of all HCN channels (15, 16), increasing intracellular cAMP induced repetitive firing of FCM neurons and suggested a possible mechanism of firing and seizure induction different from the traditional excitatory input-induced firing mechanism. HCN4 was also found in dysmorphic cortical neurons from patients with TSC and FCDII who underwent surgery for epilepsy treatment. Finally, using a genetic approach to block HCN4 activity in FCM neurons prevented seizures in the mouse model. Collectively, our findings identified a potential mechanism responsible for seizure generation in mTOR-dependent FCM and suggest that a targeted gene therapy treatment option to prevent seizure initiation might be effective in reducing seizures in TSC and FCDII.

Results

Silencing FCM neurons decreases seizure activity in mice

To investigate the mechanisms of seizure generation in FCM, we used a mouse model that recapitulates the focal nature of the cortical malformation and the cellular mosaicism of human FCDII and TSC brains (14, 17). To generate this model, we used in utero electroporation (IUE) to induce mTOR hyperactivity in pyramidal neurons in a limited cortical area (Fig. 1A) (14, 17–21). IUE at embryonic day (E) 15 specifically targets radial glia that generate layer 2/3 pyramidal neurons (Fig. 1B). To increase mTOR activity, we expressed a constitutively active mutant Rheb ($Rheb^{CA}$), the canonical mTOR activator (18, 20, 22–24) (Fig. 1B). A green or red fluorescent protein (GFP or tdTomato) was co-expressed to label neurons. These mice developed a singular FCM in the medial prefrontal cortex (Fig. 1C) that displayed a pathology resembling that of human FCM, including the presence of misplaced and cytomegalic $Rheb^{CA}$-expressing neurons that are interchangeably called FCM neurons (Fig. 1D). Whereas control GFP-expressing neurons are located in layer 2/3, FCM neurons are scattered across cortical layers 2-to-5 (Fig. 1E). In addition, FCM neurons showed an increase in soma size and immunoreactivity for phosphorylated protein S6 (phospho-S6), a read-out of mTOR activity, compared to control neurons in mice electroporated with GFP only (Fig. 1F–H). Mice containing FCM were visually observed to develop convulsive seizures by postnatal day (P) 21. To better characterize the seizures, we obtained epidural electroencephalography (EEG) recordings combined with video monitoring for 5–7 consecutive days in 3–4 months old mice. Mice containing FCM exhibited recurrent, Racine grade 4–5 seizures with classical interictal, tonic, clonic, and postictal periods (Fig. 1I and J, and movie S1; seizure frequency and duration are shown in subsequent figures).

Using our mouse model of FCM, we previously reported that FCM neurons display depolarized resting membrane potentials (RMP) compared to their control counterparts and are therefore closer to the threshold for generating action potentials (18). We thus examined whether silencing FCM neurons without normalizing their morphological abnormalities, which could contribute to seizure generation, would limit the incidence of seizures. To do this, we overexpressed inwardly rectifying potassium channels 2.1 (Kir2.1) that are expected to hyperpolarize neurons and decrease their membrane resistances (25). Using E15 IUE, we co-expressed Kir2.1 with $Rheb^{CA}$ (Fig. 2A). In the control condition, GFP was co-electroporated with $Rheb^{CA}$. Kir2.1 expression in $Rheb^{CA}$ neurons did not prevent the formation of FCM (Fig. 2A and B) and did not interfere with mTOR hyperactivity as shown by quantification of soma size and phospho-S6 immunofluorescence, respectively (Fig. 2C). Furthermore, patch clamp recordings of $Rheb^{CA}$ neurons in acute slices from P26 to P42 validated that Kir2.1 expression did not alter membrane capacitance (a read-out of soma size), but significantly hyperpolarized $Rheb^{CA}$ neurons and increased their membrane conductance ($P<0.05$ and <0.01, Student's t-test, respectively, Fig. 2D). The properties of current-induced action potentials, including half-width and threshold, were unaltered by Kir2.1 expression (Fig. 2E and F), but consistent with the changes in RMP and membrane conductance, larger current injections were required for the generation of action potentials in Kir2.1-expressing FCM neurons that resulted in a shift in the input (injected current

amplitude)-output (number of action potentials) curve (Fig. 2G, H). Thus, expressing Kir2.1 rendered FCM neurons less excitable, in part via hyperpolarizing their RMP further away from the action potential threshold. Mice overexpressing Kir2.1 in FCM neurons displayed a significant decrease in seizure frequency (from a mean of 4.5 to 0.5 seizures per day, $P<0.01$, Student's t-test) without affecting seizure duration (Fig. 2I and J). Collectively, these data suggest that alterations in the electrical properties of FCM neurons are involved in seizure initiation and that silencing these neurons is sufficient to reduce the number of seizures in mice.

FCM neurons abnormally express HCN channels leading to depolarized RMP and cAMP sensitivity

We next examined the electrical properties of FCM neurons using patch clamp recordings in acute brain slices from P26-P42 mice. As we previously reported, we confirmed that FCM neurons displayed significantly depolarized RMP and increased conductance compared to control neurons in littermate mice expressing only GFP ($P<0.0001$, Student's t-test, Fig. 3A and B) (21). Consistent with an increased conductance, there was a shift in the input (injected current from their RMP)-output (# of action potentials) curve, suggesting that $Rheb^{CA}$ neurons are less likely to generate action potentials upon depolarizations (Fig. 3C and D). Using hyperpolarizing current step, we noticed a robust "sag" response in $Rheb^{CA}$ neurons that was either minimal or mostly not present in control neurons (Fig. 3E and G) (26). Such a sag response suggests the presence of HCN channels. Under control conditions, HCN channels are primarily expressed in deep but not in superficial (2–3) layer neurons (26), which are the neuronal population targeted by IUE at E15. In addition, HCN-mediated currents are known to control neuron RMP and may contribute to the depolarized RMP in $Rheb^{CA}$ neurons (15, 16, 27). Therefore, we preferentially focused on these channels. To validate that these sags were due to the presence of HCN channels, we recorded $Rheb^{CA}$ neurons in the presence of the HCN channel blocker, zatebradine. Zatebradine reduced the sag response in $Rheb^{CA}$ neurons (Fig. 3F and G). Using voltage clamp, we applied 500-ms-long hyperpolarizing voltage steps (from −40 to −130 mV) to activate HCN channels (Fig. 3H). $Rheb^{CA}$ neurons displayed large hyperpolarization-activated inward currents that were much larger than in the control neurons (Fig. 3, H and I). These inward currents displayed a slow activation kinetics resembling that of HCN-mediated currents (called h currents), which required a 3-s-long voltage pulse to reach full amplitude (fig. S1), and were reduced in the presence of zatebradine (Fig. 3, H and I). However, zatebradine did not fully block the increased hyperpolarization-induced inward currents. This is likely due to an increase in the amplitude of inwardly rectifying K currents (Kir) in $Rheb^{CA}$ neurons compared to control, which accompanies the increase in cell size. As observed on the current–membrane potential curves (Fig. 3H), zatebradine shifted RMP of cells to hyperpolarized values that were similar to the RMP of control neurons (Fig. 3J and see Fig. 3A). This effect is consistent with a functional block of HCN channels. To quantify the h current amplitudes, we measured the amplitude difference (ΔI) between the onset and the end of the current trace using a 500-ms-long voltage step (see dotted line and Ih in Fig. 3H). Zatebradine significantly reduced ΔI [$P < 0.001$ at −80 mV and $P < 0.0001$ at −90 and up, two-way repeated measures analysis of variance (ANOVA) followed by Tukey posttest; Fig. 3K]. In addition, there was no residual inward current at −90 mV, consistent with the lack of Kir currents at this voltage (Fig. 3K).

Throughout the rest of the manuscript, Ih current amplitude will then be measured as ΔI at −90 mV. Consistent with the normalization of RMP with zatebradine, larger h currents were associated with more depolarized RMPs in Rheb^{CA} neurons (Fig. 3L). The amplitude of the h currents was also dependent on the amount of electroporated Rheb^{CA} plasmid and, thus, the degree of mTOR activation (fig. S1). HCN channels contribute to the generation of rhythmic firing in neurons and heart cells (27, 28) and display different sensitivity to intracellular cAMP concentrations (15, 16). We thus examined whether increasing cAMP in Rheb^{CA} neurons would be sufficient to trigger spontaneous, repetitive firing independent of depolarizations. We bath-applied a well-characterized cell-permeable adenylate cyclase activator, forskolin, to increase intracellular cAMP in acute brain slices containing Rheb^{CA} neurons. When recorded at RMP, all Rheb^{CA} neurons were depolarized by forskolin and 4/9 neurons generated repetitive action potentials (Fig. 3, M and N). This effect did not occur in control superficial layer neurons (layer 2/3; Fig. 3, M and N), which express very few or no HCN channels.

Ectopic HCN4 expression in FCM neurons

HCN channels are encoded by four genes, *HCN1–4*, with different expression patterns throughout the brain (15). In the adult cortex, deep layer pyramidal neurons predominantly express HCN1 and display low HCN2 expression (30). HCN3 and HCN4 display weak, diffuse expression in the cortex thought to arise from subcortical projections and HCN4 expression has recently been found in neuronal cell bodies scattered in the cortex that may be GABAergic neurons (30–32). Consistent with the previous finding on HCN1 and HCN2 (30), we observed HCN1 staining in presumed apical dendrites of deep layer neurons and weak, diffuse HCN2 staining in the cortex (Fig. 4A and). However, we found no changes in HCN1 and HCN2 staining pattern in the ipsilateral cortex containing FCM compared to the contralateral cortex of 2-month old mice (Fig. 4A, B, and E, and Fig. S2A and B). We found no HCN3 staining in the cortex and no change between ipsilateral and contralateral cortex (Fig. 4E and S2C). However, we identified strong HCN4 immunostaining in the cortex containing Rheb^{CA} neurons that was higher than that in the contralateral cortex (Fig. 4C–E). he increase in HCN4 channel expression in the ipsilateral versus contralateral cortex suggests that aberrant HCN channel expression does not result from recurrent seizures. About 83% of Rheb^{CA} neurons displayed HCN4 immunoreactivity that decorated their soma, dendrites, and axons (N=4 mice, Fig. 4F and G. One of the HCN4 antibodies (Alomone Labs) was previously validated in conditional knockout mice (31). The specificity of both HCN4 antibodies was further confirmed by siRNA-mediated HCN4 knockdown in vitro (Fig. S3). Further, these antibodies showed immunoreactivity in pyramidal neurons electroporated with an HCN4 overexpression plasmid, and not in the surrounding non-electroporated cells (Fig. S4). Finally, GFP-expressing cells in mice electroporated with GFP instead of Rheb^{CA} did not display HCN4 expression (Fig. 4H and I). Thus, Rheb^{CA}-expressing neurons display selective HCN4 expression that was absent in control pyramidal neurons.

Abnormal HCN4 expression is mTOR-dependent and precedes seizure onset

To assess whether increased mTOR activity was responsible for the abnormal expression of HCN4, we treated mice with the mTOR inhibitor rapamycin using the treatment paradigm

(1 mg/kg every 48 hours from P1 to 2 months of age) that prevented FCM and the development of seizures (14). Rapamycin treatment prevented the expression of HCN4 in Rheb^{CA} neurons compared to vehicle-treated mice (Fig. 5A–C). mTOR is a master regulator of protein translation, but can also lead to increases in mRNA. Therefore, we examined whether *Hcn4* mRNA was increased in Rheb^{CA}- compared to GFP-electroporated cortices from 3–4 month-old mice. Quantitative RT-PCR was performed for *Hcn1,2*, and *4,* as well as *Vegf*, which is increased in hyperactive mTOR conditions (33, 34). The expression of *Hcn1*, *2* and *4* mRNA were unchanged whereas the expression of *Vegf* mRNA was significantly increased ($P<0.05$, Student's t-test, Fig. 5D). Considering that HCN channel expression has been shown to be up- or down-regulated by seizures (35), we examined whether Rheb^{CA} neurons would express HCN channels during postnatal cortical development prior to the onset of convulsive seizures, which were visible in >P21 mice. Recordings in slices from P8-P12 mice showed that Rheb^{CA} neurons displayed zatebradine-sensitive Ih currents that were greater than in control GFP neurons recorded in littermate mice ($P<0.001$ at −90 mV and <0.0001 at −100 to −130 mV, two-way repeated measures ANOVA followed by Tukey's post-test, Fig. 5E–G). In addition, there was a significant increase in Ih currents in Rheb^{CA} neurons during development from P6–12 to P28-P42 ($P<0.0001$, one way ANOVA), but no change in control neurons (Fig. 5H). These data indicate that mTOR hyperactivity participate in the aberrant expression of HCN4 in FCM neurons prior to the onset of convulsive seizures.

HCN4 is abnormally expressed in human TSC and FCDII neurons.

Data presented above indicate that HCN4 channels confer a spiking advantage in Rheb^{CA} neurons that otherwise would not be able to generate repetitive firing upon cAMP stimulation. To examine whether abnormal HCN4 expression occurs in patients with FCM, we obtained cortical tissue from nine patients that underwent surgery for epilepsy due to FCM. Details about the samples (patient age, sex, fixation type, and medical notes) as well as the staining performed are summarized in Table S1. Seven patients had the histopathological diagnosis of FCDII and two patients had TSC. Patients had FCM detected on magnetic resonance imaging (MRI) and underwent EEG with a combination of subdural grid and depth electrodes prior to FCM resection. Patients were identified as FCDII post-surgery based on pathological examination of the hematoxylin-stained resected tissue and identification of hallmarks of FCDII, including cortical dyslamination and the presence of cytomegalic neurons. In all the samples (N=7 FCDII and 2 TSC), we performed HCN4 immunostaining and observed enlarged cells with strong HCN4 immunoreactivity (Figs. 6 and 7, and Figs. S5–S7, Neuromab and Alomone antibodies in all 9 samples and in 3 frozen samples, respectively). Upon quantification, HCN4-positive cells displayed increased soma size compared to normal-appearing, surrounding cells that had no or weak HCN4 staining (Fig. 6E and F, mean of 15–53 analyzed cells per sample, N=7 hematoxylin-stained samples). HCN4-positive fibers were visible in 6/9 samples (Fig. 6) and may correspond to either processes of diseased neurons or thalamic inputs or both (36). In three frozen samples (2 FCDII and 1 TSC), we co-immunostained for HCN4 and phospho-S6 (Fig. 6G and H, Fig. S7A–C, and Fig. 7A–C). HCN4-positive cells displayed increased phospho-S6 compared to surrounding cells (Fig. 7D, 13–14 cells analyzed per sample). In addition, in three frozen samples used for immunofluorescence (N=2 FCDII and 1 TSC),

we co-immunostained for SMI-311, which is a pan-neuronal neurofilament (NF) that is accumulated in the soma and dendrites of dysmorphic neurons in human and murine FCD and is considered a marker of these neurons (10, 14, 37) (Fig. 6E and S7D–F for FCDII; Fig. 7E and F for TSC). Every HCN4-positive cell was immunoreactive for SMI-311, identifying them as dysmorphic neurons (n=7–15 cells/sample). Collectively, these data show that both mouse FCM neurons and dysmorphic human neurons from TSC and FCDII patients display abnormal expression of HCN4 channels.

Overexpressing HCN4 in control neurons does not lead to convulsive seizures

We next examined whether ectopic expression of HCN4 alone was sufficient to trigger convulsive seizures (28, 29, 38, 39). To do so, we expressed a plasmid encoding HCN4 together with tdTomato or GFP using IUE at E15 to target layer 2/3 neurons. As reported above, HCN4 antibodies detected HCN4 immunostaining selectively in pyramidal neurons electroporated with HCN4 plasmid (Fig. S4). Neurons overexpressing HCN4 were located in layer 2/3 as in control condition and did not display increased soma size or increased phospho-S6 staining compared to contralateral layer 2/3 neurons (Fig. S8A–C). In acute slices of P21–43 mice, HCN4-overexpressing neurons displayed larger hyperpolarization-activated inward currents and mean depolarized RMP compared to control neurons (Fig. S8D–F). HCN4-overexpressing neurons display a mean input-output (# of action potentials) curve similar to that of control neurons although firing is detected earlier (Fig. S8G and H). We next performed 7-day long video-EEG recordings of mice expressing HCN4 channels. None of the HCN4-expressing mice displayed tonic-clonic seizures (n=7/7, Fig. S8K). Nonetheless, 5/7 mice displayed epileptiform discharges containing spikes, spike trains, or waves (defined in (40)) that were absent in GFP-expressing mice (Fig. S8I–K). These data show that HCN4 overexpression in control pyramidal neurons of the medial prefrontal cortex (mPFC) without morphological alterations typical of $Rheb^{CA}$ neurons was not sufficient to trigger convulsive seizures.

Blocking HCN4 activity prevents the establishment of epilepsy.

To then address whether the ectopic expression of HCN4 channels in $Rheb^{CA}$ neurons contributed to seizure generation in FCM-expressing mice, we blocked HCN channel activity in vivo. To do so, we expressed nonfunctional HCN4 ($HCN4^{NF}$) subunits that were generated by adding two mutations into *HCN4* (41). $HCN4^{NF}$ subunits are expected to form heteromers with endogenous HCN4 subunits and render the endogenous HCN4 channel unable to conduct ions, thus acting as dominant-negative. Indeed, both the sag responses observed in current clamp and the h currents recorded in voltage clamp in $Rheb^{CA}$ neurons were eliminated in $Rheb^{CA}$ neurons that co-expressed $HCN4^{NF}$ (Fig. 8A and B). Furthermore, $HCN4^{NF}$ expression hyperpolarized the RMP of $Rheb^{CA}$ neurons (Fig. 8C) similarly to what was shown with the HCN channel blocker zatebradine in Figure 3. Similar to the experiments with Kir2.1, expressing $HCN4^{NF}$ in $Rheb^{CA}$ neurons did not interfere with mTOR hyperactivity as measured by phospho-S6 immunofluorescence and soma size (Fig. 8D and E). $HCN4^{NF}$ expression in $Rheb^{CA}$ neurons did not alter the properties of action potentials (Fig. 8F) or the input-output curve (Fig. 8G and H). Thus, expressing $HCN4^{NF}$ in $Rheb^{CA}$ neurons did not alter their ability to generate actions potentials, but it blocked the activity of endogenous HCN4 channels and hyperpolarized the RMP.

Finally, a 7-day long continuous video-EEG monitoring of mice containing Rheb^{CA} neurons expressing HCN4^{NF} revealed that these mice had no seizures whereas littermate mice containing Rheb^{CA} neurons (without HCN4^{NF}) displayed a mean of three daily, convulsive seizures (Fig. 8I and J). Together, these data indicate that the abnormal expression of HCN4 channels in FCM neurons is necessary for generating seizures and blocking HCN4 channels is sufficient to decrease seizure activity.

Discussion

To examine whether Rheb^{CA} neurons may be hyperexcitable and thus trigger seizures, we expressed Kir2.1 channels in Rheb^{CA} neurons to hyperpolarize them (18). Kir2.1 expression indeed hyperpolarized Rheb^{CA} neurons and increased their membrane conductance leading to a right shift in the input-output curve without preventing increased cell size, mTOR hyperactivity, and misplacement in mice. Rheb^{CA} neurons expressing Kir2.1 were thus less excitable and less responsive to depolarization. As a result of this manipulation, mice had fewer seizures, suggesting that alterations in Rheb^{CA} neurons' electrical properties contribute to seizures. Using patch clamp recordings to examine electrical properties, we confirmed that Rheb^{CA} neurons have depolarized RMP and are thus closer to the threshold for generating action potentials. However, they also displayed increased conductance and required a larger depolarizing current injection to reach firing threshold. Therefore, Rheb^{CA} neurons are less responsive to depolarization than control neurons. These findings seemed to contradict the conclusion from the Kir2.1 experiment suggesting that Rheb^{CA} neurons should not trigger seizures. However, we identified the aberrant expression of HCN-mediated currents, which provided an explanation for the increased likelihood of Rheb^{CA} neurons to generate action potentials independent of depolarizing inputs, but dependent upon intracellular cAMP concentrations as further detailed below. In young adult mice, Rheb^{CA} neurons expressed larger inward currents than in controls, including a combination of HCN- and presumed Kir-mediated currents. Outward currents could not be examined in Rheb^{CA} mouse neurons due to unclamped firing upon depolarizing voltage pulses. Due to the large increase in Rheb^{CA} neuron size, it was not surprising to find larger Kir-mediated currents, which are expressed in control layer 2/3 pyramidal neurons (42, 43). However, finding HCN-mediated currents was surprising because control layer 2/3 pyramidal neurons do not express such currents, as confirmed here. HCN channels, in particular HCN2 and HCN4, are sensitive to intracellular cAMP concentrations with higher concentrations leading to increased HCN-mediated currents (15, 16). Considering that the concentrations of cAMP increases in developing hippocampal neurons (44) and could be altered in disease condition, it is conceivable that the increase in HCN-mediated currents could also be due to increased cAMP concentrations in Rheb^{CA} neurons. We could not directly measure cAMP concentrations in Rheb^{CA} neurons. However, using immunostaining we identified the selective expression of HCN4 that was not present in control neurons and expressing HCN4^{NF} led to a reduction of HCN-mediated currents. These data suggest that HCN-mediated currents in Rheb^{CA} neurons are primarily due to the ectopic expression of HCN4 channels independent of changes in cAMP concentrations. Increasing intracellular cAMP concentrations with forskolin was sufficient to trigger the firing of Rheb^{CA} neurons. Therefore, although Rheb^{CA} neurons have an increased membrane conductance and require

more current injection to reach firing threshold, they are more depolarized and thus closer to the firing threshold, and an increase in intracellular cAMP concentrations, as opposed to excitatory input-induced depolarization, could act as the trigger to induce Rheb^{CA} neuron firing. These data show an unanticipated mechanism of excitability that is consistent with a decrease in the excitatory drive (onto Rheb^{CA} neurons (18). Cortical pyramidal neurons receive multiple inputs (including, noradrenergic and dopaminergic innervation from the locus coeruleus (45) and the ventral tegmental area (43, 46)) that activate receptors leading to cAMP increases. Noradrenaline or dopamine released from these inputs could thus increase cAMP and activate HCN4 channels that would lead to firing and seizures. It is conceivable that preventing aberrant increases in cAMP, through inhibition of these specific receptors, might contribute to reduce seizure activity.

Among the different HCN channels, we found the selective expression of HCN4 channels in Rheb^{CA} neurons. HCN4 expression was absent in control pyramidal neurons in our sections consistent with previous reports showing no expression in cortical pyramidal neurons in adult mice despite the presence of mRNA (30–32, 47, 48). Finding HCN4 channels in neurons that normally do not express these channels may seem surprising. However, as shown in the developing hippocampus (44, 49), HCN4 channels are expressed perinatally in the cortex and are dramatically decreased in young adults (P30) (32). Considering HCN4 expression was mTOR-dependent, and mTOR increases protein translation, it is conceivable that the ectopic HCN4 expression results from increased translation of mRNA already present in pyramidal neurons. Consistent with this idea is the lack of changes in *Hcn4* mRNA expression in Rheb^{CA}- neurons. This is also consistent with the lack of changes in *Hcn4* mRNA expression in gene arrays performed in cortical tuber samples from individuals with TSC (50–52).

Our findings add to a large body of literature on HCN expression and seizures. Several studies have reported alterations in the expression of HCN, in particular, HCN1 and HCN2, in different types of epilepsy in both mice and humans (for review (35, 53)). (54) Regarding HCN4 channels, a study reported no change in HCN4 expression in the hippocampus following febrile seizures despite changes in HCN1 (55). However, loss-of-function mutations in HCN4 have been associated with benign myoclonic epilepsy (56) and increased HCN4 expression in the hippocampal dentate gyrus has been reported in individuals with sudden unexpected death (57). Nevertheless, it was unclear whether the alterations in HCN4 expression preceded seizure occurrence or were responsible for seizures. Here, we identified the abnormal expression of HCN-mediated currents in Rheb^{CA} neurons as early as P8, about two weeks prior to the onset of convulsive seizures (observed starting at P21). In addition, HCN4 expression was not detected in the contralateral hemispheres lacking FCM, but experiencing epileptiform activity. Overexpression of HCN4 channels in control layer 2/3 pyramidal neurons was not sufficient to cause convulsive seizures despite depolarizing them. However, expressing nonfunctional HCN4 channels in Rheb^{CA} neurons that act as dominant negative prevented seizures. These data show that HCN4 channels in FCM neurons are necessary for seizures. The lack of convulsive seizure generation with HCN4 channel expression is not surprising considering that FCM neurons display an array of alterations, such as increased dendrite complexity and axon lengths (16, 21, 23). Thus, our data suggest that a combination of alterations is required for seizures,

but blocking one single alteration, such as ectopic HCN4 expression or increased filamin A expression (58) is sufficient to prevent seizures.

Identifying ectopic HCN4 has several important clinical implications. At the present time, there are no HCN blockers that are selective for HCN4. However, our findings support HCN4 as a prime candidate for short hairpin RNA-based gene therapy for treating seizures associated with FCDII and TSC that exhibit focal cortical malformations. While ectopic HCN4 expression was eliminated with rapamycin treatment, directly targeting HCN4 for epilepsy treatment would prevent the severe adverse events that occur when using the higher rapamycin doses necessary to improve efficacy (6). Furthermore, considering that HCN4 is downstream of mTOR signaling, our findings are likely applicable to other mTORopathies resulting from mutations in the mTOR and GATOR pathway genes (59).

We acknowledge several limitations to our study. First, we did not use a dual construct containing $Rheb^{CA}$ and Kir2.1-mCherry or HCN4. A few cells will thus express Kir2.1-mCherry or HCN4 without expressing $Rheb^{CA}$. Could these cells contribute to the decrease in seizures? This is unlikely for the following reason. The co-electroporated vectors are expressed in the same cell type, layer 2/3 pyramidal neurons, and ~92% of the electroporated neurons will colocalize both plasmids (60). Considering that IUE targets about 10% of layer 2/3 neurons, we do not anticipate that silencing 0.8% of layer 2/3 control neurons intermingled with $Rheb^{CA}$ neurons would be sufficient to prevent seizures. In the case of $HCN4^{NF}$, the control layer 2/3 pyramidal neurons do not express HCN and as such the expression of nonfunctional channels is like expressing channelrhodopsin, which has no impact on the cell biophysics. Second, although we found that the increase in HCN4 (protein) is mTOR-dependent and there is no increase in its mRNA, the mechanisms leading to this increase remains unknown. It is, however, possible that a small increase in *Hcn4* mRNA was not detectable in microdissected tissue. Third, although it has been shown that blocking another molecular player, filamin A, can reduce seizures in adults (58), it remains to be examined whether blocking HCN4 activity in adults once epilepsy is established can also reduce seizures. Fourth, our seizure data are only acquired using a mouse model of the TSC. It is unknown whether data obtained in mice would be applicable to humans. Nevertheless, considering that our mouse model recapitulates the pathological features observed in humans (17, 18, 20, 22, 24), and the increase in HCN4 is also observed in the cortices of patients with TSC and FCDII, we hope that our seizure data will be applicable to humans. Finally, it is essential to assess whether viral delivery of an shRNA against *Hcn4* would reduce seizures without leading to brain inflammation. It would be preferential to express the shRNA selectively in pyramidal neurons using specific promoter to avoid targeting interneurons, some of which may express HCN4, and validate that the viral vector infects diseased neurons. In addition, it will be necessary to assess whether one or multiple viral injections are required to cover the cortical malformations and assess how many diseased neurons need to be infected to reduce seizures.

In conclusion, we have provided evidence that enlarged, dysmorphic mutant neurons in mouse and human FCMs express HCN4 channels that are normally absent in cortical neurons in adults. In mice, this ectopic HCN4 channel expression is mTOR-dependent, precedes the development of epilepsy, and contributes to the generation of seizures by

depolarizing FCM neurons that are then closer to the firing threshold and by enhancing their cAMP-dependent excitability. Our findings add to the body of literature on HCN channels in epilepsy and highlight a possible mechanism of seizures in mice that involves HCN4 channels that have high cAMP-sensitivity. This mechanism might help to explain how sensory stimulations leading to the activation of cAMP-generating dopaminergic or adrenergic inputs onto FCM neurons would trigger seizures. In addition, the unique expression of HCN4 channels in dysmorphic FCM neurons provides a potential target for reducing seizures in TSC and FCDII.

Materials and Methods

Details of the methods are provided in the Supplementary material.

Study Design

Our research objective was to investigate whether, and if so how, FCM neurons contributed to seizure generation in our mouse model of TSC/FCD. We have extensive experience with the mouse model that we developed that is based on using IUE of $Rheb^{CA}$. To assess whether FCM neurons could contribute to seizures, we expressed selective ion channels, Kir2.1 to hyperpolarize FCM neurons. After finding that Kir2.1 indeed hyperpolarized FCM neurons and decreased seizure frequency, we obtained whole cell patch clamp recordings to assess the biophysics of FCM neurons. Using patch recordings followed by immunostaining, we identified the expression of HCN4 in FCM neurons. Antibodies were validated with siRNA in cell lines. The Alomone lab was validated by other labs. To then block the activity of HCN4 channels, we expressed nonfunctional HCN4 channels that acted as dominant negative, which was validated with patch clamp recordings. Experimental and control animals were littermate although several litters had to be used for most experiments, and none were excluded from analysis at the time of harvest. Experimental animals were lost prior to or during seizure recordings either due to sudden death by seizure or due to technical issues with the recording system. No attempt was made to segregate results based on gender or sex. Analysis was performed blindly and seizure analysis was performed by two investigators. Blinding was performed at multiple points during the experiments. For example, after video-EEG recording, the recording files were renamed for analysis by investigators blinded to the treatment condition.

Normality was checked with D'Agostino And Pearson normality test, and reported in Data File S1. Sample sizes were estimated based on our previous experience both for assessing neuronal biophysical properties and seizure activity. The sample size calculation was performed using power analysis with G*Power 3 (61). For each set of experiment, the sample size was estimated for an effect size of 50–70% using SD calculated from the control population and a power at 0.8 (β=0.2) and an α of 0.05. Each experiment was reproduced at least three times with n greater or equal to three as detailed in Table S4. We removed one outlier in Fig. 2F using Grubbs' test as indicated in Data File S1. There was no impact on statistical results (no significant differences). The brain of every recorded mouse was examined post-EEG recording to make sure that the mouse with no seizure had proper electroporation. Raw data are reports as separate excel document in Datafile S1.

Statistical analyses

All analyses were conducted blindly knowing only the arbitrarily assigned animal ID (independent of electroporation condition). Statistical tests and plots were performed using Prism 7 (GraphPad Software, Inc.), with $P < 0.05$ for significance for all experiments. Specific statistical tests used for each experiment are described in Table S4. Data are presented as mean ± SEM.

Supplementary Material

Refer to Web version on PubMed Central for supplementary material.

Acknowledgments:

We thank Drs. Stieber and Ludwig (Institute of Experimental and Clinical Pharmacology and Toxicology, Erlangen, Germany) for the pcDNA3-hHCN4 plasmid and Drs. Hanada and Maehama (National Institute of Infectious Diseases) for the $Rheb^{CA}$ plasmid.

Funding:

This work was supported by NIH/NINDS R21 NS093510 (AB), DoD TS150058 (AB), R01 NS111980 (AB), the Swebilius Foundation (AB), Brown Coxe Postdoctoral Fellowship (LHN), American Epilepsy Society Postdoctoral Fellowship (LHN), NIH/NICHD F32 HD095567 (LHN), and National Natural Science Foundation of China 81671123 (LZ). We thank the Tuberous Sclerosis Alliance for providing one TSC sample.

References

1. Leventer RJ, Guerrini R, Dobyns WB, Malformations of cortical development and epilepsy. Dialogues Clin Neurosci 10, 47–62 (2008). [PubMed: 18472484]
2. Crino PB, Focal Cortical Dysplasia. Semin Neurol 35, 201–208 (2015). [PubMed: 26060899]
3. Najm IM, Sarnat HB, Blumcke I, Review: The international consensus classification of Focal Cortical Dysplasia - a critical update 2018. Neuropathol Appl Neurobiol 44, 18–31 (2018). [PubMed: 29359399]
4. Wong-Kisiel LC, Blauwblomme T, Ho ML, Boddaert N, Parisi J, Wirrell E, Nabbout R, Challenges in managing epilepsy associated with focal cortical dysplasia in children. Epilepsy Res 145, 1–17 (2018). [PubMed: 29803953]
5. Zhang K, Hu WH, Zhang C, Meng FG, Chen N, Zhang JG, Predictors of seizure freedom after surgical management of tuberous sclerosis complex: a systematic review and meta-analysis. Epilepsy Res 105, 377–383 (2013). [PubMed: 23523658]
6. French JA, Lawson JA, Yapici Z, Ikeda H, Polster T, Nabbout R, Curatolo P, de Vries PJ, Dlugos DJ, Berkowitz N, Voi M, Peyrard S, Pelov D, Franz DN, Adjunctive everolimus therapy for treatment-resistant focal-onset seizures associated with tuberous sclerosis (EXIST-3): a phase 3, randomised, double-blind, placebo-controlled study. Lancet 388, 2153–2163 (2016). [PubMed: 27613521]
7. Stevelink R, Sanders MW, Tuinman MP, Brilstra EH, Koeleman BP, Jansen FE, Braun KP, Epilepsy surgery for patients with genetic refractory epilepsy: a systematic review. Epileptic Disord 20, 99–115 (2018). [PubMed: 29620010]
8. Iffland PH 2nd, Crino PB, Focal Cortical Dysplasia: Gene Mutations, Cell Signaling, and Therapeutic Implications. Annu Rev Pathol 12, 547–571 (2017). [PubMed: 28135561]
9. Wong M, Mammalian target of rapamycin (mTOR) activation in focal cortical dysplasia and related focal cortical malformations. Exp Neurol 244, 22–26 (2013). [PubMed: 22015915]
10. Wang Y, Greenwood JS, Calcagnotto ME, Kirsch HE, Barbaro NM, Baraban SC, Neocortical hyperexcitability in a human case of tuberous sclerosis complex and mice lacking neuronal expression of TSC1. Ann. Neurol 61, 139–152 (2007). [PubMed: 17279540]

11. Abdijadid S, Mathern GW, Levine MS, Cepeda C, Basic mechanisms of epileptogenesis in pediatric cortical dysplasia. CNS Neurosci Ther 21, 92–103 (2015). [PubMed: 25404064]
12. Kannan L, Vogrin S, Bailey C, Maixner W, Harvey AS, Centre of epileptogenic tubers generate and propagate seizures in tuberous sclerosis. Brain 139, 2653–2667 (2016). [PubMed: 27497492]
13. Major P, Rakowski S, Simon MV, Cheng ML, Eskandar E, Baron J, Leeman BA, Frosch MP, Thiele EA, Are cortical tubers epileptogenic? Evidence from electrocorticography. Epilepsia 50, 147–154 (2009). [PubMed: 19125835]
14. Hsieh LS, Wen JH, Claycomb K, Huang Y, Harrsch FA, Naegele JR, Hyder F, Buchanan GF, Bordey A, Convulsive seizures from experimental focal cortical dysplasia occur independently of cell misplacement. Nat. Commun 7, 11753 (2016). [PubMed: 27249187]
15. Robinson RB, Siegelbaum SA, Hyperpolarization-activated cation currents: from molecules to physiological function. Annu Rev Physiol 65, 453–480 (2003). [PubMed: 12471170]
16. Benarroch EE, HCN channels: function and clinical implications. Neurology 80, 304–310 (2013). [PubMed: 23319474]
17. Nguyen LH, Mahadeo T, Bordey A, mTOR Hyperactivity Levels Influence the Severity of Epilepsy and Associated Neuropathology in an Experimental Model of Tuberous Sclerosis Complex and Focal Cortical Dysplasia. J Neurosci, (2019).
18. Lin TV, Hsieh L, Kimura T, Malone TJ, Bordey A, Normalizing translation through 4E-BP prevents mTOR-driven cortical mislamination and ameliorates aberrant neuron integration. Proc. Natl. Acad. Sci. U. S. A 113, 11330–11335 (2016). [PubMed: 27647922]
19. Feliciano DM, Su T, Lopez J, Platel JC, Bordey A, Single-cell Tsc1 knockout during corticogenesis generates tuber-like lesions and reduces seizure threshold in mice. J. Clin. Invest 121, 1596–1607 (2011). [PubMed: 21403402]
20. Gong X, Zhang L, Huang T, Lin TV, Miyares L, Wen J, Hsieh L, Bordey A, Activating the translational repressor 4E-BP or reducing S6K-GSK3beta activity prevents accelerated axon growth induced by hyperactive mTOR in vivo. Hum. Mol. Genet 24, 5746–5758 (2015). [PubMed: 26220974]
21. Zhang L, Huang T, Teaw S, Bordey A, Hypervascularization in mTOR-dependent focal and global cortical malformations displays differential rapamycin sensitivity. Epilepsia 60, 1255–1265 (2019). [PubMed: 31125447]
22. Hsieh LS, Wen J, Claycomb K, Huang Y, Harrsch FA, Naegele JR, Hyder F, Buchanan GF, Bordey A, Convulsive seizures from experimental focal cortical dysplasia occur independently of cell misplacement. Nature Communications, In Press (2016).
23. Lafourcade CA, Lin TV, Feliciano DM, Zhang L, Hsieh LS, Bordey A, Rheb activation in subventricular zone progenitors leads to heterotopia, ectopic neuronal differentiation, and rapamycin-sensitive olfactory micronodules and dendrite hypertrophy of newborn neurons. J. Neurosci 33, 2419–2431 (2013). [PubMed: 23392671]
24. Zhang L, Bartley CM, Gong X, Hsieh LS, Lin TV, Feliciano DM, Bordey A, MEK-ERK1/2-Dependent FLNA Overexpression Promotes Abnormal Dendritic Patterning in Tuberous Sclerosis Independent of mTOR. Neuron 84, 78–91 (2014). [PubMed: 25277454]
25. Xue M, Atallah BV, Scanziani M, Equalizing excitation-inhibition ratios across visual cortical neurons. Nature 511, 596–600 (2014). [PubMed: 25043046]
26. Albertson AJ, Williams SB, Hablitz JJ, Regulation of epileptiform discharges in rat neocortex by HCN channels. J Neurophysiol 110, 1733–1743 (2013). [PubMed: 23864381]
27. Gasparini S, DiFrancesco D, Action of the hyperpolarization-activated current (Ih) blocker ZD 7288 in hippocampal CA1 neurons. Pflugers Arch 435, 99–106 (1997). [PubMed: 9359908]
28. Pape HC, McCormick DA, Noradrenaline and serotonin selectively modulate thalamic burst firing by enhancing a hyperpolarization-activated cation current. Nature 340, 715–718 (1989). [PubMed: 2475782]
29. Herrmann S, Hofmann F, Stieber J, Ludwig A, HCN channels in the heart: lessons from mouse mutants. Br J Pharmacol 166, 501–509 (2012). [PubMed: 22141457]
30. Notomi T, Shigemoto R, Immunohistochemical localization of Ih channel subunits, HCN1–4, in the rat brain. J. Comp Neurol 471, 241–276 (2004). [PubMed: 14991560]

31. Zobeiri M, Chaudhary R, Blaich A, Rottmann M, Herrmann S, Meuth P, Bista P, Kanyshkova T, Luttjohann A, Narayanan V, Hundehege P, Meuth SG, Romanelli MN, Urbano FJ, Pape HC, Budde T, Ludwig A, The Hyperpolarization-Activated HCN4 Channel is Important for Proper Maintenance of Oscillatory Activity in the Thalamocortical System. Cereb Cortex 29, 2291–2304 (2019). [PubMed: 30877792]
32. Battefeld A, Rocha N, Stadler K, Brauer AU, Strauss U, Distinct perinatal features of the hyperpolarization-activated non-selective cation current I(h) in the rat cortical plate. Neural Dev 7, 21 (2012). [PubMed: 22694806]
33. Feliciano DM, Zhang S, Quon JL, Bordey A, Hypoxia-inducible factor 1a is a Tsc1-regulated survival factor in newborn neurons in tuberous sclerosis complex. Hum. Mol. Genet 22, 1725–1734 (2013). [PubMed: 23349360]
34. Parker WE, Orlova KA, Heuer GG, Baybis M, Aronica E, Frost M, Wong M, Crino PB, Enhanced epidermal growth factor, hepatocyte growth factor, and vascular endothelial growth factor expression in tuberous sclerosis complex. Am. J. Pathol 178, 296–305 (2011). [PubMed: 21224066]
35. Noam Y, Bernard C, Baram TZ, Towards an integrated view of HCN channel role in epilepsy. Curr. Opin. Neurobiol 21, 873–879 (2011). [PubMed: 21782415]
36. Cruikshank SJ, Ahmed OJ, Stevens TR, Patrick SL, Gonzalez AN, Elmaleh M, Connors BW, Thalamic control of layer 1 circuits in prefrontal cortex. J Neurosci 32, 17813–17823 (2012). [PubMed: 23223300]
37. Blumcke I, Aronica E, Miyata H, Sarnat HB, Thom M, Roessler K, Rydenhag B, Jehi L, Krsek P, Wiebe S, Spreafico R, International recommendation for a comprehensive neuropathologic workup of epilepsy surgery brain tissue: A consensus Task Force report from the ILAE Commission on Diagnostic Methods. Epilepsia 57, 348–358 (2016). [PubMed: 26839983]
38. Stieber J, Herrmann S, Feil S, Loster J, Feil R, Biel M, Hofmann F, Ludwig A, The hyperpolarization-activated channel HCN4 is required for the generation of pacemaker action potentials in the embryonic heart. Proc Natl Acad Sci U S A 100, 15235–15240 (2003). [PubMed: 14657344]
39. Abbas SY, Ying SW, Goldstein PA, Compartmental distribution of hyperpolarization-activated cyclic-nucleotide-gated channel 2 and hyperpolarization-activated cyclic-nucleotide-gated channel 4 in thalamic reticular and thalamocortical relay neurons. Neuroscience 141, 1811–1825 (2006). [PubMed: 16806719]
40. Kane N, Acharya J, Benickzy S, Caboclo L, Finnigan S, Kaplan PW, Shibasaki H, Pressler R, van Putten M, A revised glossary of terms most commonly used by clinical electroencephalographers and updated proposal for the report format of the EEG findings. Revision 2017. Clin Neurophysiol Pract 2, 170–185 (2017). [PubMed: 30214992]
41. Mesirca P, Alig J, Torrente AG, Muller JC, Marger L, Rollin A, Marquilly C, Vincent A, Dubel S, Bidaud I, Fernandez A, Seniuk A, Engeland B, Singh J, Miquerol L, Ehmke H, Eschenhagen T, Nargeot J, Wickman K, Isbrandt D, Mangoni ME, Cardiac arrhythmia induced by genetic silencing of 'funny' (f) channels is rescued by GIRK4 inactivation. Nat. Commun 5, 4664 (2014). [PubMed: 25144323]
42. Saenz del Burgo L, Cortes R, Mengod G, Zarate J, Echevarria E, Salles J, Distribution and neurochemical characterization of neurons expressing GIRK channels in the rat brain. J Comp Neurol 510, 581–606 (2008). [PubMed: 18698588]
43. Radnikow G, Feldmeyer D, Layer- and Cell Type-Specific Modulation of Excitatory Neuronal Activity in the Neocortex. Front Neuroanat 12, 1 (2018). [PubMed: 29440997]
44. Surges R, Brewster AL, Bender RA, Beck H, Feuerstein TJ, Baram TZ, Regulated expression of HCN channels and cAMP levels shape the properties of the h current in developing rat hippocampus. Eur J Neurosci 24, 94–104 (2006). [PubMed: 16882011]
45. Chandler DJ, Gao WJ, Waterhouse BD, Heterogeneous organization of the locus coeruleus projections to prefrontal and motor cortices. Proc Natl Acad Sci U S A 111, 6816–6821 (2014). [PubMed: 24753596]
46. Grzelka K, Kurowski P, Gawlak M, Szulczyk P, Noradrenaline Modulates the Membrane Potential and Holding Current of Medial Prefrontal Cortex Pyramidal Neurons via beta1-Adrenergic Receptors and HCN Channels. Front Cell Neurosci 11, 341 (2017). [PubMed: 29209170]

47. Monteggia LM, Eisch AJ, Tang MD, Kaczmarek LK, Nestler EJ, Cloning and localization of the hyperpolarization-activated cyclic nucleotide-gated channel family in rat brain. Brain Res. Mol. Brain Res 81, 129–139 (2000). [PubMed: 11000485]
48. Moosmang S, Biel M, Hofmann F, Ludwig A, Differential distribution of four hyperpolarization-activated cation channels in mouse brain. Biol. Chem 380, 975–980 (1999). [PubMed: 10494850]
49. Brewster AL, Chen Y, Bender RA, Yeh A, Shigemoto R, Baram TZ, Quantitative analysis and subcellular distribution of mRNA and protein expression of the hyperpolarization-activated cyclic nucleotide-gated channels throughout development in rat hippocampus. Cereb Cortex 17, 702–712 (2007). [PubMed: 16648453]
50. Martin KR, Zhou W, Bowman MJ, Shih J, Au KS, Dittenhafer-Reed KE, Sisson KA, Koeman J, Weisenberger DJ, Cottingham SL, DeRoos ST, Devinsky O, Winn ME, Cherniack AD, Shen H, Northrup H, Krueger DA, MacKeigan JP, The genomic landscape of tuberous sclerosis complex. Nat Commun 8, 15816 (2017). [PubMed: 28643795]
51. Mills JD, van Vliet EA, Chen BJ, Janitz M, Anink JJ, Baayen JC, Idema S, Devore S, Friedman D, Diehl B, Thom M, Scott C, Thijs R, Aronica E, Devinsky O, Coding and non-coding transcriptome of mesial temporal lobe epilepsy: Critical role of small non-coding RNAs. Neurobiol Dis 134, 104612 (2020). [PubMed: 31533065]
52. Boer K, Crino PB, Gorter JA, Nellist M, Jansen FE, Spliet WG, van Rijen PC, Wittink FR, Breit TM, Troost D, Wadman WJ, Aronica E, Gene expression analysis of tuberous sclerosis complex cortical tubers reveals increased expression of adhesion and inflammatory factors. Brain Pathol 20, 704–719 (2010). [PubMed: 19912235]
53. Reid CA, Phillips AM, Petrou S, HCN channelopathies: pathophysiology in genetic epilepsy and therapeutic implications. Br. J. Pharmacol 165, 49–56 (2012). [PubMed: 21615728]
54. David F, Carcak N, Furdan S, Onat F, Gould T, Meszaros A, Di Giovanni G, Hernandez VM, Chan CS, Lorincz ML, Crunelli V, Suppression of Hyperpolarization-Activated Cyclic Nucleotide-Gated Channel Function in Thalamocortical Neurons Prevents Genetically Determined and Pharmacologically Induced Absence Seizures. J Neurosci 38, 6615–6627 (2018). [PubMed: 29925625]
55. Brewster A, Bender RA, Chen Y, Dube C, Eghbal-Ahmadi M, Baram TZ, Developmental febrile seizures modulate hippocampal gene expression of hyperpolarization-activated channels in an isoform- and cell-specific manner. J Neurosci 22, 4591–4599 (2002). [PubMed: 12040066]
56. Campostrini G, DiFrancesco JC, Castellotti B, Milanesi R, Gnecchi-Ruscone T, Bonzanni M, Bucchi A, Baruscotti M, Ferrarese C, Franceschetti S, Canafoglia L, Ragona F, Freri E, Labate A, Gambardella A, Costa C, Gellera C, Granata T, Barbuti A, DiFrancesco D, A Loss-of-Function HCN4 Mutation Associated With Familial Benign Myoclonic Epilepsy in Infancy Causes Increased Neuronal Excitability. Front Mol Neurosci 11, 269 (2018). [PubMed: 30127718]
57. Papanicolou MB, A; C Moore, P15-T increased HCN4 expression in hippocampus of SUDEP patients. Clinical Neurophysiology 130.
58. Zhang L, Huang T, Teaw S, Nguyen LH, Hsieh LS, Gong X, Burns LH, Bordey A, Filamin A inhibition reduces seizure activity in a mouse model of focal cortical malformations. Sci Transl Med 12, (2020).
59. Iffland PH 2nd, Carson V, Bordey A, Crino PB, GATORopathies: The role of amino acid regulatory gene mutations in epilepsy and cortical malformations. Epilepsia 60, 2163–2173 (2019). [PubMed: 31625153]
60. Hartman NW, Lin TV, Zhang L, Paquelet GE, Feliciano DM, Bordey A, mTORC1 Targets the Translational Repressor 4E-BP2, but Not S6 Kinase 1/2, to Regulate Neural Stem Cell Self-Renewal In Vivo. Cell Rep 5, 433–444 (2013). [PubMed: 24139800]
61. Faul F, Erdfelder E, Lang AG, Buchner A, G*Power 3: a flexible statistical power analysis program for the social, behavioral, and biomedical sciences. Behav Res Methods 39, 175–191 (2007). [PubMed: 17695343]
62. Racine RJ, Modification of seizure activity by electrical stimulation. II. Motor seizure. Electroencephalogr. Clin. Neurophysiol 32, 281–294 (1972). [PubMed: 4110397]

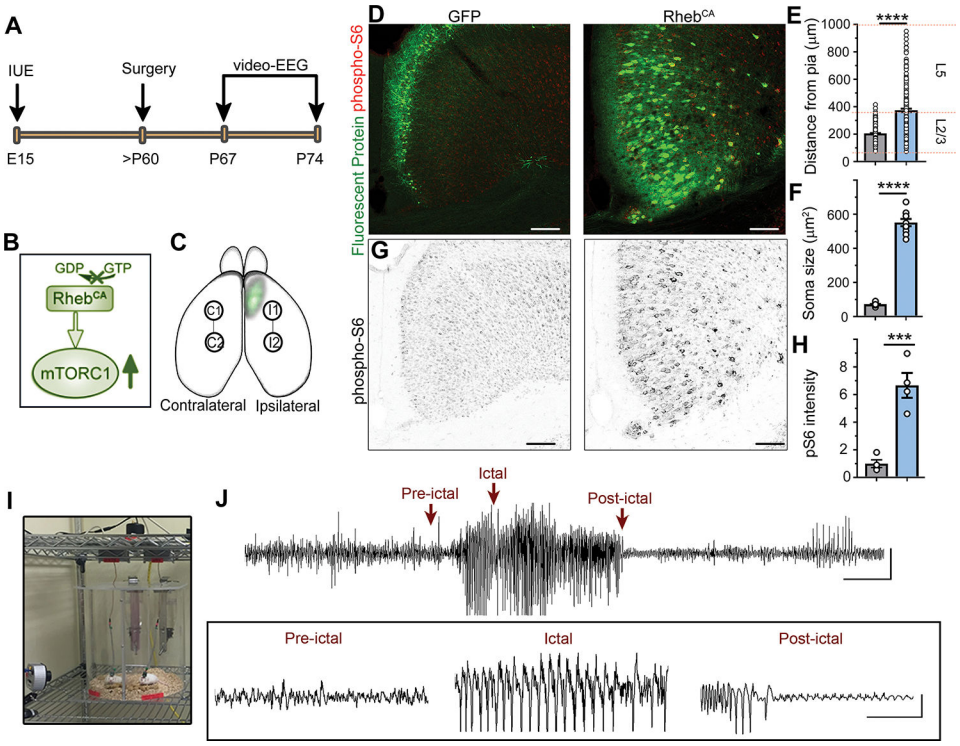

Figure 1: Model of mTOR-dependent FCM-associated seizures.

(A) Timeline of the experimental paradigm. **(B)** Diagram of Rheb^{CA} effect on mTOR complex 1 (mTORC1). **(C)** Diagram of a mouse brain with superimposed image of a FCM in the medial prefrontal cortex (mPFC). Linked circles mark the approximate locations of independent pairs of recording electrodes in the ipsilateral and contralateral hemispheres. **(D)** Confocal images of GFP and tdTomato (pseudo-colored green) fluorescence and phospho-S6 immunostaining (red) in coronal sections from 3 month-old mice expressing GFP (control) or Rheb^{CA} (+ tdTomato) in the mPFC. Scale bars: 150 µm. **(E and F)** Bar graphs of the distance from pia surface (E) and soma size (F) of GFP- and Rheb^{CA}-expressing neurons. **(G)** B&W phospho-S6 immunostaining from images shown in D. Scale bar: 150 µm. **(H)** Bar graphs of phospho-S6 (pS6) immunofluorescence in GFP and Rheb^{CA}-expressing neurons. **(I)** Image of the video-EEG set-up. **(J)** Representative examples of an EEG trace and higher temporal resolution traces in the inset. Scale bars: 10 s/200 µV and 2 s/200 µV (inset). Data are mean ± SEM. ***: P<0.001, ****: P<0.0001, ns: not significant. Statistical analysis: MannWhitney U test (E), Student's t test (F and G). Exact *P* values can be found in Table S4.

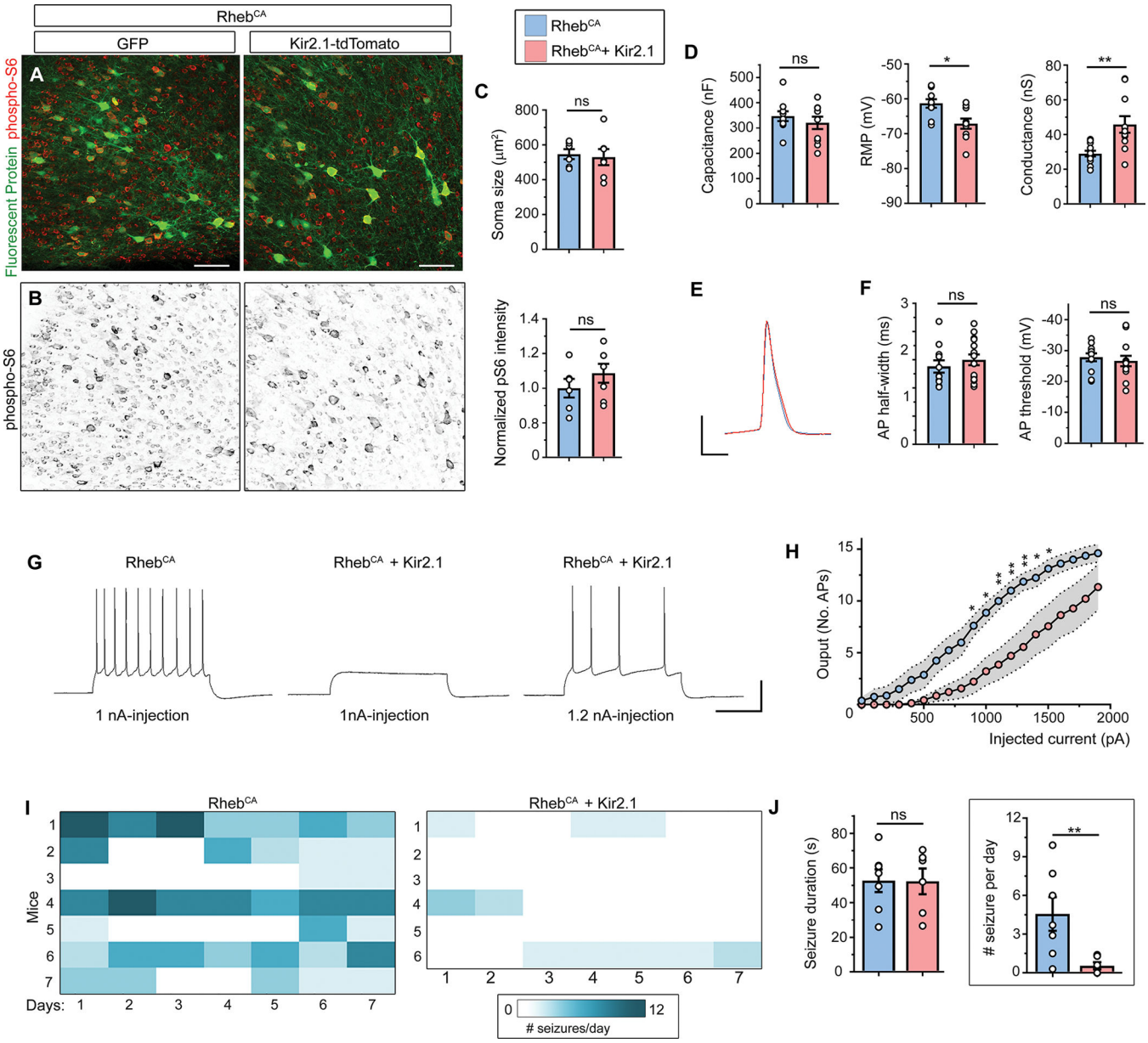

Figure 2: Silencing cytomegalic neurons in mTOR-driven FCM prevents seizure activity.

(A) Confocal images of GFP and tdTomato fluorescence (pseudo-colored green) and phospho-S6 immunostaining (red) in coronal sections from 4 month-old littermate mice (used in panel J) expressing Rheb^{CA} + GFP or + Kir2.1 (fused to tdTomato). Scale bar: 100 µm. **(B)** B&W phospho-S6 immunostaining from images shown in A. **(C)** Bar graphs of normalized phospho-S6 immunofluorescence intensity and soma size of Rheb^{CA} neurons co-expressing GFP (green) or Kir2.1 (pink). **(D)** Bar graphs of cell capacitance, resting membrane potential (RMP), and membrane conductance of Rheb^{CA} neurons co-expressing GFP or Kir2.1. Patch clamp recordings were obtained in acute slices from P26-P42 mice. **(E)** Superimposed individual action potentials from Rheb^{CA} neurons in both conditions. Scale bars: 2 ms/40 mV. **(F)** Bar graphs of the action potential (AP) half-width and threshold. **(G)** Representative depolarization and action potentials upon current injection in

Rheb^{CA} co-expressing GFP or Kir2.1. Scales: 200 ms/40 mV. **(H)** Injected current amplitude against the mean number of action potentials for generating an input-output curve in Rheb^{CA} neurons. The grey area outlines the SEM for each curve. **(I)** Heat map of the number of seizures over a 7-day long recording period in mice containing Rheb^{CA} neurons with GFP or Kir2.1. **(J)** Bar graphs of the duration and number of seizures per day in the two conditions. Statistical analyses: Student's t test (C, D, F, and J, seizure frequency), Two-way repeated measure ANOVA, followed by Sidak post-test (H), and Mann Whitney U test (J, seizure duration). Data are mean ± SEM. *: P<0.05, **: P<0.01, ***: P<0.001, ****: P<0.0001, ns: not significant. Exact *P* values can be found in Table S4.

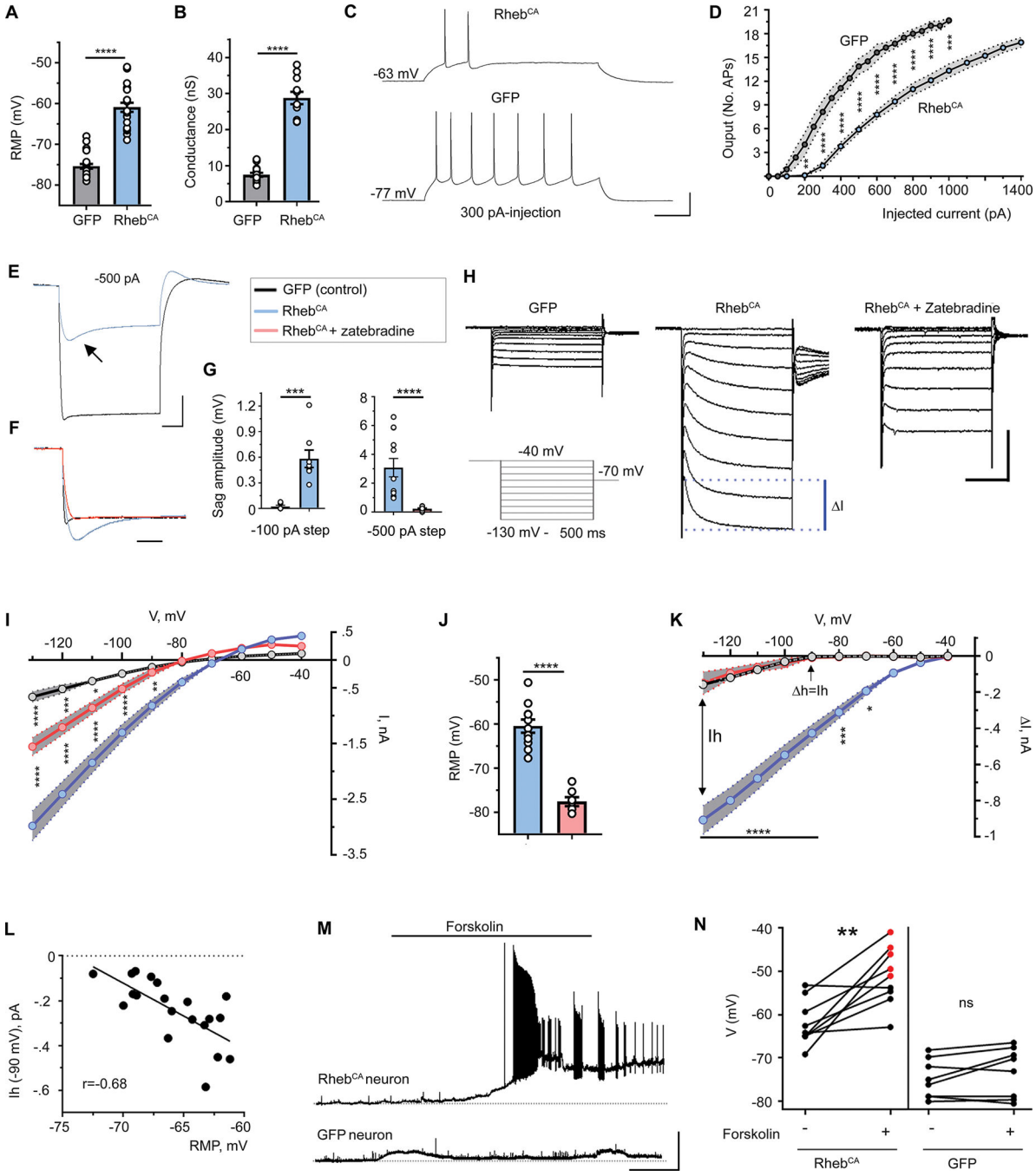

Figure 3: Abnormal HCN-mediated currents in FCM neurons are depolarizing and confer cAMP-dependent firing.

(A and B) Bar graphs of the RMP and conductance of control (GFP) and Rheb^{CA} neurons recorded in littermate P26-P42 mice. **(C)** Representative depolarization and action potentials upon current injection in Rheb^{CA} or control (GFP) neurons. Scales: 100 ms/40 mV. **(D)** Injected current amplitude plotted as a function of the mean number of action potentials for generating an input-output curve in Rheb^{CA} neurons. The grey area outlines the SEM for each curve. **(E)** Representative voltage traces in response to a −500 pA step in neurons

expressing GFP (black) or Rheb^{CA} (green). Neurons were recorded in current-clamp at their RMP and voltage traces were superimposed post-recording. The arrow points to a hyperpolarization-induced voltage sag. Scales: 100 ms/10 mV. **(F)** Voltage traces in response to a −500 pA step from GFP-expressing neurons (black), Rheb^{CA}-expressing neurons (green), and Rheb^{CA}-expressing neurons in the presence of zatebradine (40 μM, red). Voltage responses were rescaled and superimposed post-recording. Scale: 100 ms. **(G)** Plots of the sag amplitude following a −100 pA from GFP or Rheb^{CA} neurons (left) or a −500 pA step protocol from Rheb^{CA} neurons under vehicle or zatebradine condition (right). (H) Representative current traces in cortical GFP or Rheb^{CA} neurons with vehicle or zatebradine. Protocol: conditioning step to −40 mV followed by 10 mV-hyperpolarizing steps from −130 to −40 mV. Scale bars: 200 ms/1 nA. The blue dotted lines illustrate where the difference in current amplitude (ΔI) was measured within each voltage step to generate current-voltage (ΔI-V) curves in K. **(I)** Current amplitude (I, measured at the end of the trace) versus the voltage in each condition. The grey area indicates the SEM for each curve. **(J)** Bar graphs of the RMP for each condition. **(K)** ΔI-V curves. At −90 mV, ΔI corresponds to Ih. Statistics is for Rheb^{CA} vs Rheb^{CA} + zatebradine. **(L)** Scatter plot of Ih (measured at −90 mV) against the RMP. Two-tailed Pearson r with correlation coefficients. **(M and N)** Voltages traces during bath-application of forskolin on Rheb^{CA} and control neurons (M), and resulting plots of the voltage changes (N). The red dots indicate the neurons (4/9) that generated repetitive firing upon forskolin application. Scale bars: 5 min/30 mV. Data are mean ± SEM. Statistical analyses: Unpaired Student's t test (A,B, and J), Mann-Whitney U test (G), paired Student's t test (N), Two-way repeated measure ANOVA, followed by Sidak post-test (D) and by Tukey's post-test (I, K). ****:P<0.0001, ***:P<0.001, *:P<0.05, and ns: not significant. Exact *P* values can be found in Table S4.

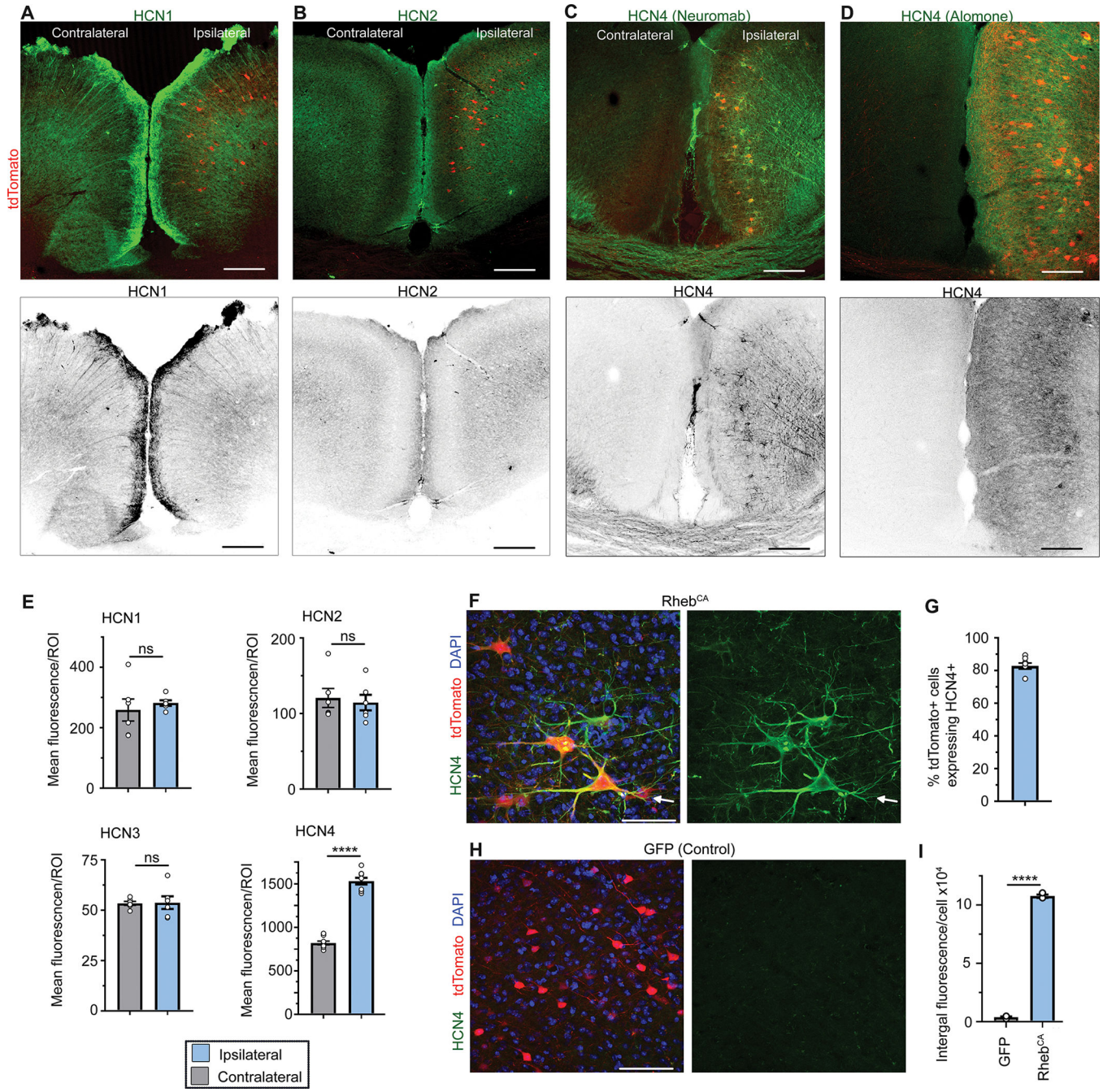

Figure 4: FCM neurons display abnormal mTOR-dependent HCN4 expression.

(A-D) Immunostaining for HCN1 (A), HCN2 (B), and HCN4 (C) in coronal sections containing Rheb^{CA} neurons co-expressing tdTomato. HCN4 staining was performed using antibodies from Neuromab and Alomone. The bottom images display HCN staining in B&W. Scale bars: 200 μm. The brain section in D was more caudal than the ones in A-C resulting in a larger cortex. In addition, 2.5 instead of 2 μg/μl of Rheb^{CA} was used. **(E)** Quantification of HCN1-HCN4 immunostaining in the ipsilateral versus contralateral cortex.. **(F)** Higher magnification images of HCN4 (green, Neuromab antibody), DAPI, and

tdTomato. Scale bar: 60 μm. **(G)** Quantification of the percentage (%) of tdTomato+ cells expressing HCN4. **(H)** Images of HCN4 immunostaining, tdTomato fluorescence and DAPI in GFP electroporated mice. Scale bar: 60 μm. **(I)** Bar graph of integral fluorescence per GFP or $Rheb^{CA}$ cell. Data are mean ± SEM. Statistical analyses: paired Student t-test (E for HCN1, 3, and 4), unpaired Student t -test (I), and Wilcoxon test (E, for HCN2), $P<0.0001$, ns: not significant.

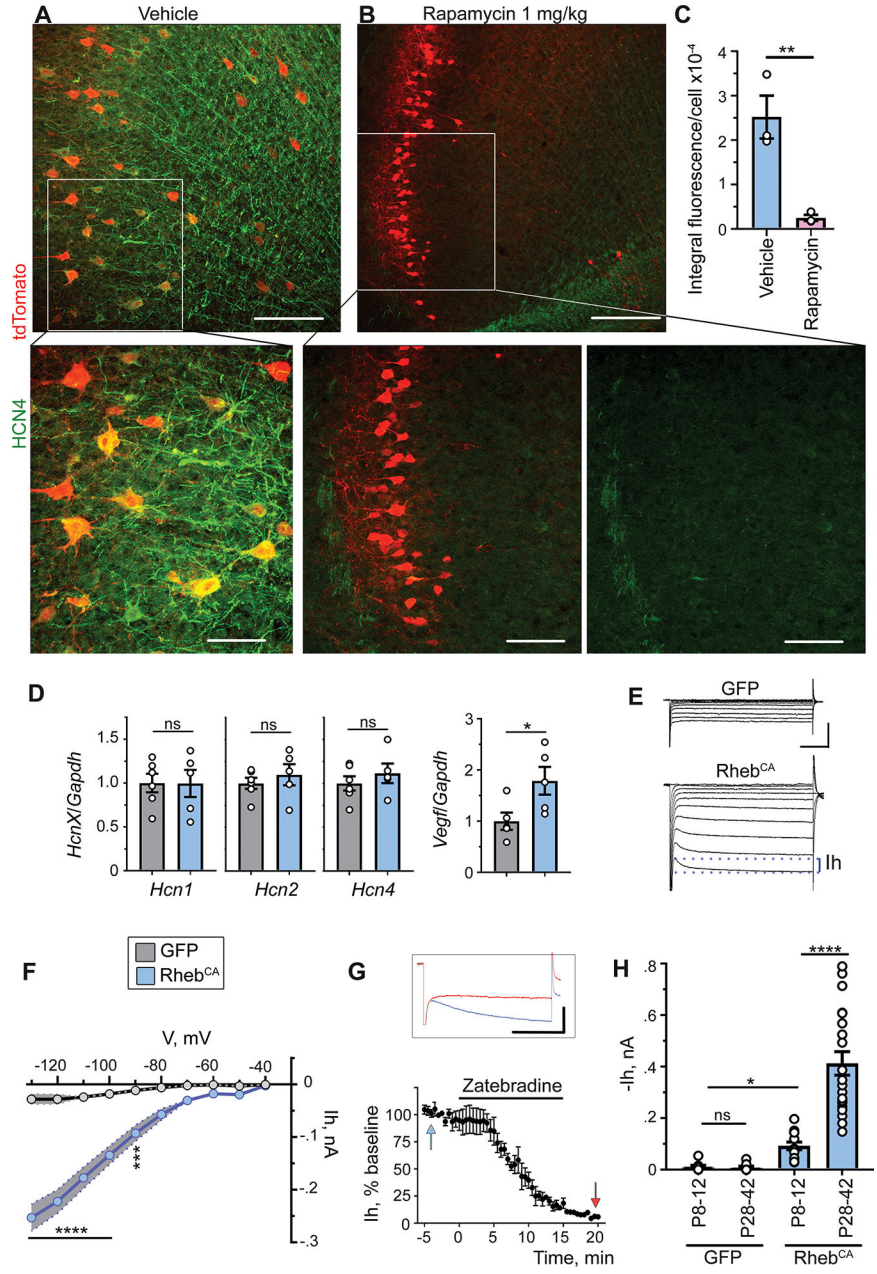

Figure 5: HCN4 expression is mTOR-dependent and precedes seizure onset.

(A and B) HCN4 immunostaining (Neuromab) and tdTomato fluorescence in Rheb^{CA} mice treated with vehicle (A) or rapamycin (B) and higher magnification images). Scale bars: 140 and 60 μm, respectively. **(C)** Integral fluorescence in cells expressing Rheb^{CA} from mice treated with vehicle or rapamycin. **(D)** Normalized qRT-PCR values for *Hcn1, 2, and 4* as well as *Vegf* divided by *Gapdh* from microdissected cortices containing GFP or Rheb^{CA}. **(E and F)** Representative current traces in P8-P12 cortical neurons expressing GFP (control) or Rheb^{CA}. Scale bars: 100 ms/500 pA. The blue dotted lines illustrate where the h current amplitude (Ih) was measured within each voltage step to generate Ih-V curves (F). **(G)** Plot of the zatebradine block of Ih (measured at −90 mV) over time in a Rheb^{CA}

neuron. Left inset: traces of Zatebradine block at −90 mV in $Rheb^{CA}$ neurons. Scale bars: 200 ms/100 pA. **(H)** Bar graphs of -Ih at the different ages under control and $Rheb^{CA}$ conditions. Statistical analyses: Unpaired Student t-test. (C), Two-way repeated measures ANOVA followed by Tukey's post-test (F), and One way ANOVA (H). Data are mean ± SEM. ****:P<0.0001, ***:P<0.001, *:P<0.05, and ns: not significant. Exact *P* values can be found in Table S4.

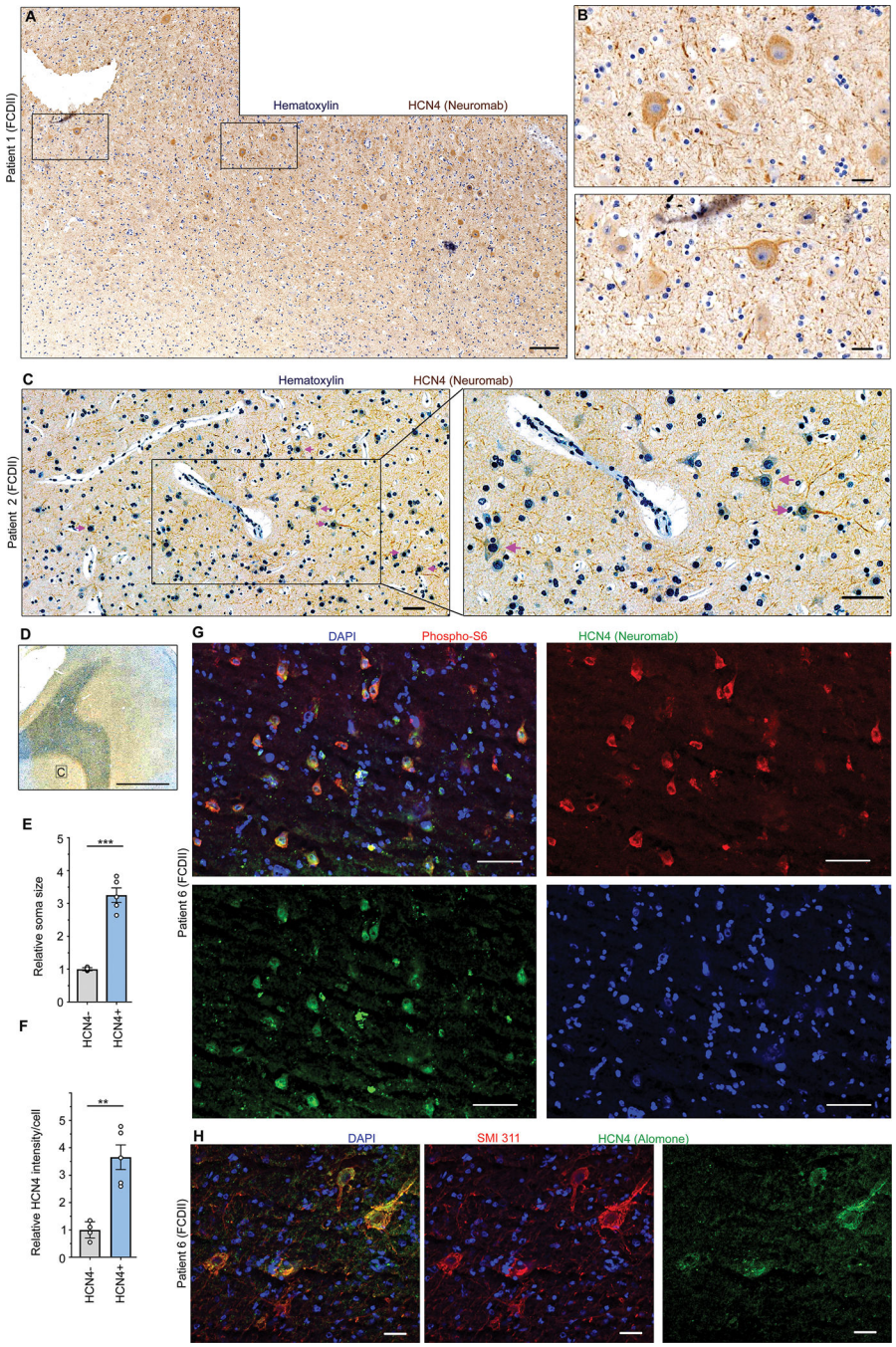

Figure 6: Ectopic HCN4 expression in diseased neurons in human FCDII cortices.

(A and B) Staining for HCN4 in patient 1 with FCDII at low (A) and high magnifications (B). Images in B was approximately from the squares in A Scale bars: 250 μm (A) and 30 μm (B). **(C)** Staining for HCN4 in patient 2 with FCDII at low and high magnifications. The pink arrows point to HCN4-positive cells. Scale bars: 250 μm and 30 μm. **(D)** Image at a lower magnification for patient 2. Scale bar: 2600 μm. **(E and F)** Relative soma size (E) and HCN4 intensity (F) in HCN4-positive and HCN4-negative cells averaged per FCDII sample. **(G and H)** Immunostaining for HCN4 and phospho-S6 (G) or SMI-311 (H) in FCDII tissue

from patient 6 co-stained with DAPI. Scale bars: 70 μm (G), 30 μm (H). Statistical analysis: paired Student t-test, ***:P<0.001, **:P<0.01.

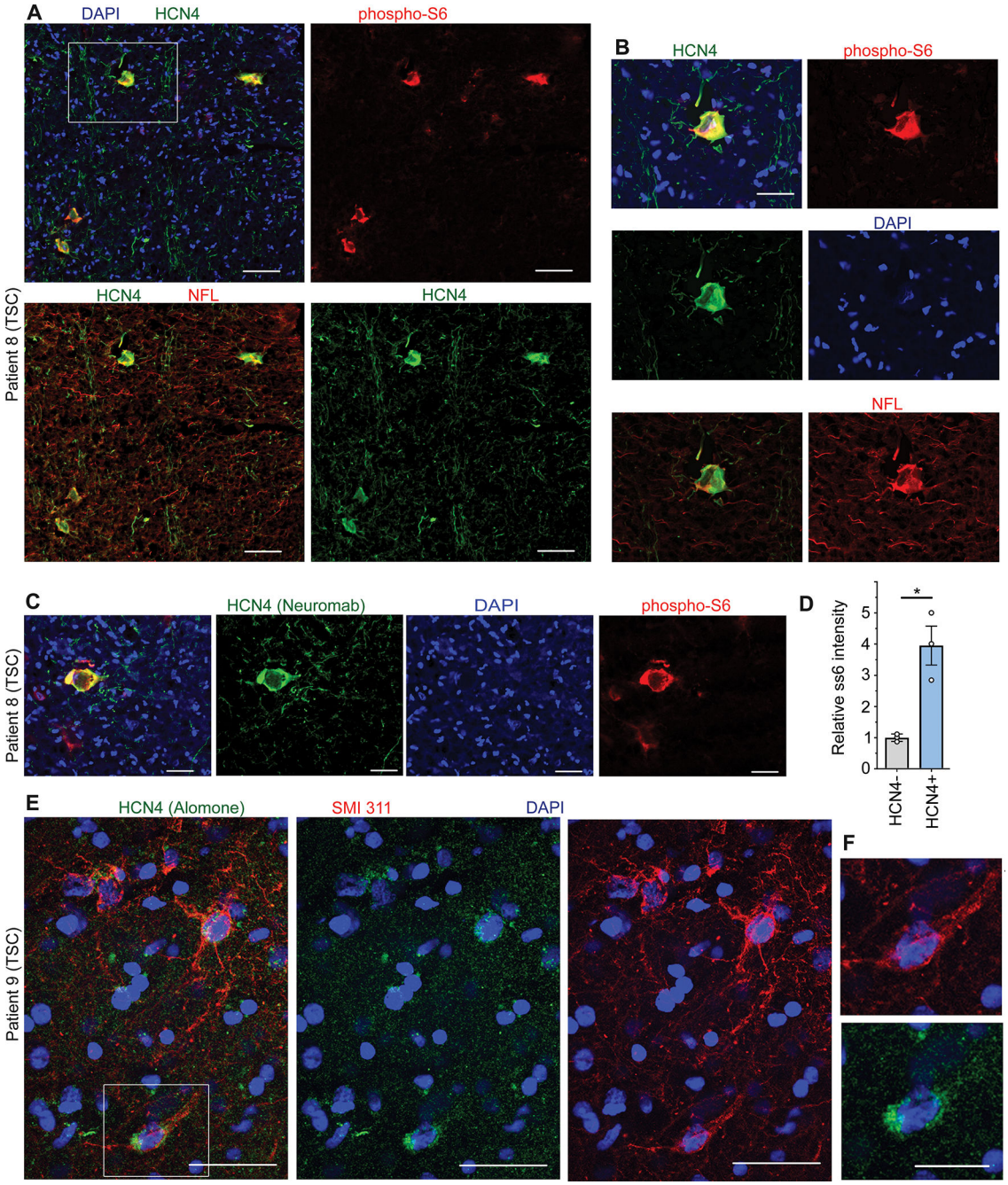

Figure 7: Ectopic HCN4 expression in diseased neurons in human TSC cortices.

(A and C) Immunostaining for HCN4 and phospho-S6 TSC tissue from patient 8 co-stained with DAPI. Scale bars: 70 μm (A) and 40 μm (C). **(B)** Higher magnification of the cell shown in the white square in A. Scale bar: 35 μm**. (D)** Quantification of phospho-S6 (pS6) intensity in HCN4+ and HCN- cells. Statistical analysis: paired Student t test. **(E)** Immunostaining for HCN4 and SMI 311 in TSC tissue from patient 9 co-stained with DAPI. Scale bar: 40 μm. **(F)** Higher magnification of the cell shown in the white square in E. Scale bar: 20 μm.

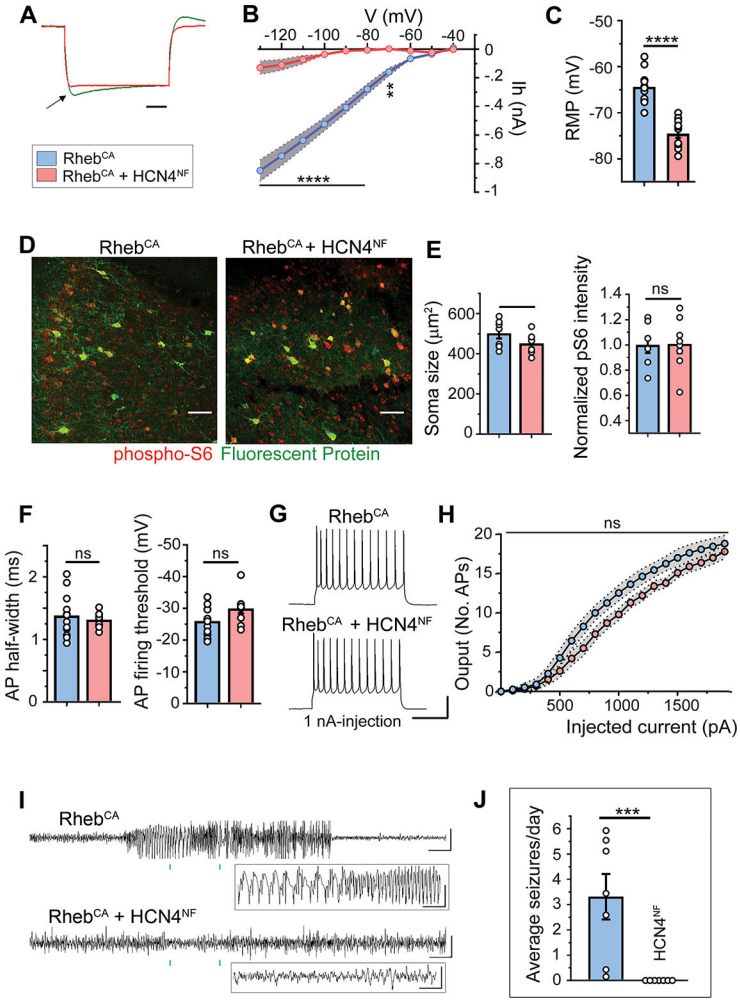

Figure 8: Blocking HCN4 channel activity in FCM neurons prevents epilepsy.

(A and B) Representative voltage-traces of Rheb^{CA} neurons with and without nonfunctional HCN4 (HCN4^{NF}) channel expression. Neurons were recorded in acute slices from P21-P35 littermate mice electroporated with Rheb^{CA}+GFP or Rheb^{CA}+HCN4^{NF} (+ tdTomato). (B) Ih-V curve in each condition. (**C**) Bar graphs of RMP. Recordings were obtained in acute slices from P21-P35 mice. (**D**) Confocal images of GFP and tdTomato fluorescence (pseudo-colored green) and phospho-S6 immunostaining (red) in coronal sections from 4 month-old mice expressing Rheb^{CA}+GFP or + HCN4^{NF} (+ tdTomato). Scale bars: 80 µm. (**E**) Bar graphs of soma size and normalized (to GFP control cells) phospho-S6 immunofluorescence for neurons expressing Rheb^{CA}+GFP or Rheb^{CA}+HCN4^{NF}. (**F**) Bar graphs of the action potential (AP) threshold and half-width. (**G**) Representative depolarization and action potentials upon current injection in Rheb^{CA} neurons with and without HCN4^{NF}. Scales: 200 ms/40 mV. (**H**) Input-output curves of Rheb^{CA} neurons with and without HCN4^{NF}. The grey area indicates the SEM for each curve. (**I**) Representative EEG traces in Rheb^{CA} mice with and without HCN4^{NF}. (**J**) Bar graphs of the number of seizures per day. Data are mean ± SEM. Statistical analyses: Two-way repeated measure ANOVA followed by Sidak post-test (B, H), Student's t test (C, E, F), and Mann Whitney U test (J). *: P<0.05, **:

P<0.01, ***: P<0.001, ****: P<0.0001, ns: not significant. Exact *P* values can be found in Table S4.